

## Near-edge x-ray absorption fine structure measurements using a laboratory-scale XUV source

This article has been downloaded from IOPscience. Please scroll down to see the full text article.

2008 J. Phys. D: Appl. Phys. 41 105202

(<http://iopscience.iop.org/0022-3727/41/10/105202>)

View [the table of contents for this issue](#), or go to the [journal homepage](#) for more

Download details:

IP Address: 134.76.163.141

The article was downloaded on 31/01/2013 at 13:15

Please note that [terms and conditions apply](#).

# Near-edge x-ray absorption fine structure measurements using a laboratory-scale XUV source

Christian Peth, Frank Barkusky and Klaus Mann

Laser-Laboratorium Göttingen e.V., Hans-Adolf-Krebs-Weg 1, D-37077 Göttingen, Germany

Received 1 February 2008, in final form 14 March 2008

Published 8 April 2008

Online at [stacks.iop.org/JPhysD/41/105202](http://stacks.iop.org/JPhysD/41/105202)

## Abstract

We present a compact setup for near-edge x-ray absorption spectroscopy at the carbon K-edge based on a laser-driven plasma source. To generate the required broad-band emission in the spectral range of the ‘water window’ ( $\lambda = 2.2\text{--}4.4\text{ nm}$ ) a krypton gas puff target was used. The table-top setup consisting basically of the laser-plasma source and a flat-field spectrometer can be used for near-edge x-ray absorption fine structure experiments in transmission as well as reflection under grazing incidence conditions (RefLEXAFS). The latter method offers the advantage that thin film preparation is not necessary and that the surface sensitivity is strongly enhanced. The results obtained for thin polymer films show good agreement with synchrotron data. Furthermore, we use the RefLEXAFS method to investigate changes in the chemical composition of PMMA induced by extreme ultraviolet (EUV) radiation. The spectra indicate a loss of the carbonyl functional group upon irradiation as well as crosslinking effects at high EUV radiation doses.

(Some figures in this article are in colour only in the electronic version)

## 1. Introduction

The progress in the development of laboratory-scale soft x-ray sources in recent years has enabled experimental techniques that could earlier be performed almost exclusively at synchrotron sources. Table-top soft x-ray sources of high brilliance, such as laser-produced plasmas [1–3], high harmonic radiation [4, 5] or x-ray lasers [6], are now used for various applications, e.g. x-ray microscopy [7, 8], lensless diffractive imaging [9], photoelectron spectroscopy [10] or absorption spectroscopy [11]. The latter, among other techniques, accomplishes the investigation of the near-edge x-ray absorption fine structure (NEXAFS). NEXAFS is a well-established method for elemental and compositional analysis of a sample yielding also surface sensitive information [12]. In particular, NEXAFS is used to study the structure of intermolecular bonds of polymers by probing the electronic transition from the core level to the unoccupied states. Since each element has a characteristic core binding energy NEXAFS spectra contain element specific information. Furthermore, the energy levels of both initial and final states are strongly dependent on the involved molecular bonds, resulting in

strong spectral features of the near-edge fine structure. The analysis of these unique spectroscopic fingerprints allows the identification and distinction of different polymers [13].

In this paper we present NEXAFS measurements that were obtained by using a laboratory-scale setup based on a laser-driven plasma source. It has already been shown that the generation of broad-band emission in the spectral range of the ‘water window’ (2.2–4.4 nm) can be achieved by using solid state targets such as gold or copper [11, 14]. Here we present a flexible setup to generate broad-band soft x-ray radiation based on a gas puff target, where new target material is supplied continuously with the advantage of low debris.

The table-top setup consisting basically only of the laser-plasma source and a flat-field spectrometer can be used for NEXAFS experiments in transmission as well as reflection under grazing incidence conditions. For transmission measurements thin films have to be used due to the low penetration depth of soft x-rays into matter. In contrast, NEXAFS experiments performed in reflection mode (RefLEXAFS) offer the advantage that thin film preparation is not necessary. Moreover, the surface sensitivity is strongly increased. We use the RefLEXAFS method to investigate

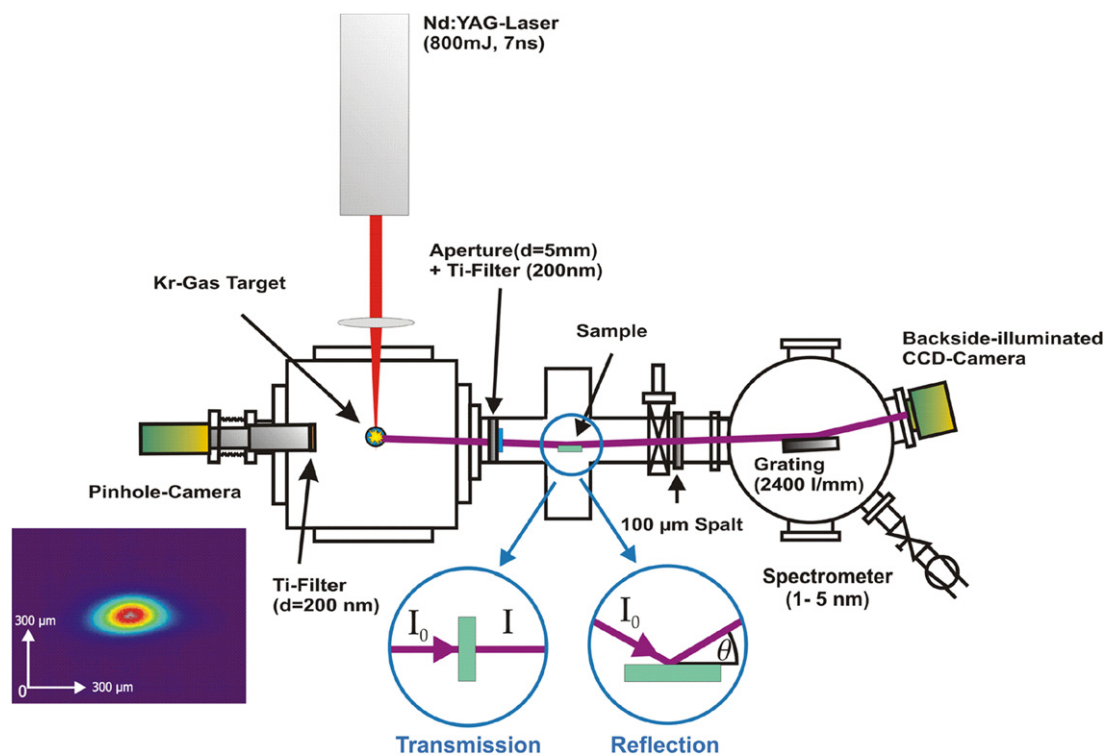


**Figure 1.** Experimental setup of the laser-plasma XUV source used for NEXAFS experiments. The setup can be used in a transmission and reflection geometry. The inset on the left shows a picture of the krypton plasma taken by the pinhole camera.

changes in the chemical composition of PMMA induced by extreme ultraviolet (EUV) radiation. The results indicate a loss of the carbonyl functional group upon irradiation, as well as crosslinking effects at high EUV radiation doses.

The use of laser-driven plasmas sources also offers the potential for time-resolved experiments in pump-probe schemes, where the same laser pulse can be used to generate a visible pump and an x-ray probe pulse.

## 2. Experimental setup

### 2.1. Laser-plasma source

The experimental setup for the generation and characterization of soft x-ray radiation emitted from laser plasmas in the ‘water window’ is shown schematically in figure 1. A Nd:YAG laser beam (Innolas, 1064 nm, 1 Hz, 800 mJ, 7 ns) is focused into a pulsed gas puff target centred in a vacuum chamber, as described in detail elsewhere [15]. The laser focus has a diameter of about  $60 \mu\text{m}$ , yielding power densities of up to  $4 \times 10^{12} \text{ W cm}^{-2}$  that are sufficient to ignite a hot and dense plasma. Krypton is employed as target gas (backing pressure 25 bar), accomplishing broad-band radiation (Kr xxv–Kr xxxvi) in the spectral range of the ‘water window’ (cf figure 3). Due to the small mean free path of the soft x-ray radiation at atmospheric pressure the target vacuum chamber is evacuated to approximately  $10^{-4}$  mbar.

The plasma can be monitored with a pinhole camera, consisting of a CCD chip with an XUV-to-VIS quantum converter and a pinhole (diameter  $30 \mu\text{m}$ ) coated with a titanium foil (thickness approximately 200 nm, average

transmission in the wavelength range from 2.71 to 6 nm  $\approx 45\%$ , 6–20 nm  $< 10\%$ ) for blocking of out-of-band radiation. The size of the krypton plasma is about  $250 \mu\text{m}$  (FWHM) in the horizontal and  $150 \mu\text{m}$  (FWHM) in the vertical direction (cf inset of figure 1).

An XUV spectrometer (1–5 nm) was used for both the spectral investigation of the plasma source and the NEXAFS experiments. The spectrometer consists of a  $100 \mu\text{m}$  entrance slit, an aberration corrected flat-field grating (Hitachi, 2400 lines  $\text{mm}^{-1}$ ) and a back-side illuminated CCD camera (Roper Scientific, pixel size  $13 \mu\text{m}$ ). The resolution of this spectrometer was experimentally determined to be  $\lambda/\Delta\lambda \approx 200$  at 2.87 nm. It was mounted  $90^\circ$  to the laser beam and opposite to the pinhole camera (cf figures 1 and 2). To block visible radiation from the plasma and scattered laser light a titanium foil (200 nm thickness) was positioned between the plasma source and the sample.

To calibrate the spectrometer nitrogen was used as target gas. The spectrum of the nitrogen plasma, ignited under the same experimental conditions as krypton, consists of several lines (e.g.  $1s^2-1s2p$  transition of N vi at 2.8787 nm [16]) that were used for spectral calibration.

For adjustment in the XUV beam the samples were mounted on a rotary/linear motion stage. The distance between the plasma source and the sample is about 220 mm and the distance between the sample and the entrance slit of the spectrometer is about 425 mm. The setup can be used for NEXAFS experiments both in transmission and in reflection mode. For the latter grazing incidence conditions are chosen ( $\theta = 2^\circ$ ).

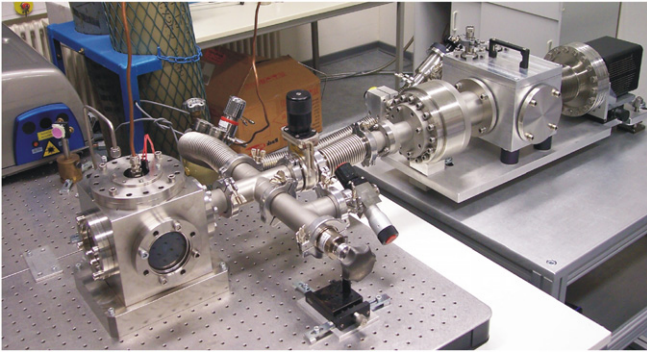


**Figure 2.** Photograph of the experimental setup of the laser-plasma XUV source and the spectrometer used for NEXAFS experiments.

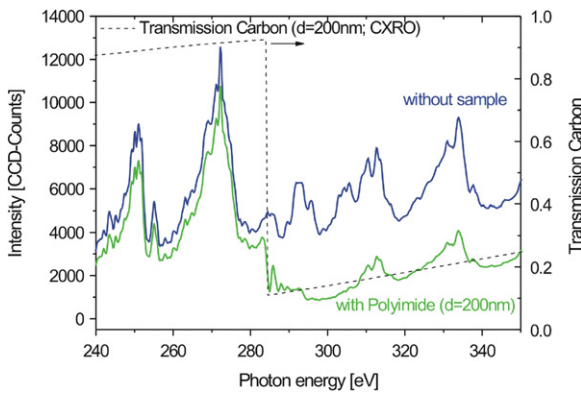


**Figure 3.** Emission spectrum of the krypton plasma with and without sample (average over 60 pulses). For comparison the calculated transmission of carbon from CXRO [17] data is shown (---).

### 3. Results and discussion

#### 3.1. NEXAFS in transmission

For thin samples it is possible to determine the x-ray absorption fine structure by measuring the transmitted flux through the sample. As an example, thin polyimide films (PI 2545, HD Microsystems,  $d = 200$  nm) were used. Figure 3 shows the emission spectra of the krypton plasma both with and without the polyimide sample, each obtained by an integration over 60 pulses (acquisition time 1 min). The transmitted spectrum clearly indicates an overall decrease in intensity above the carbon K-absorption edge.

From the data in figure 3 the optical density can be evaluated according to the Lambert–Beer law

$$\mu(E) \cdot d = -\ln\left(\frac{I}{I_0}\right), \quad (1)$$

where  $\mu(E)$  is the linear energy dependent absorption coefficient,  $d$  the sample thickness,  $I$  the transmitted and  $I_0$  the reference intensity.

Obviously, the optical density shown in figure 4 evaluated according to equation (1) features several sharp peaks below the carbon K-absorption edge which can be attributed to  $C\ 1s-\pi^*$  transitions of the benzene rings that are clearly

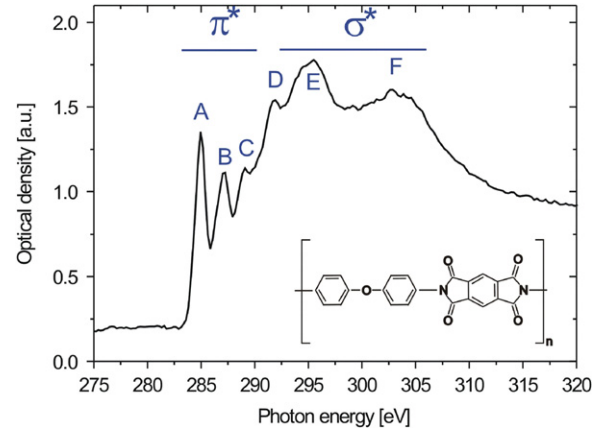


**Figure 4.** NEXAFS spectrum of polyimide film ( $d = 200$  nm), chemical structure of polyimide.

**Table 1.** Energies and assignments of features in the K-shell NEXAFS spectrum of polyimide. The reference data are taken from [18].

Feature	Energy (eV)	Assignment	Reference data (eV)
A	285.2	$1s \rightarrow \pi^*$ (C=C)	285.2
B	287.3	$1s \rightarrow \pi^*$ (C=O)	287.4
C	289.3	$1s \rightarrow \pi^*$	289.2
D	291.6	$1s \rightarrow \sigma^*$ (C–O, C–N)	291.9
E	295.0	$1s \rightarrow \sigma^*$ (C=C)	295.4
F	303.0	$1s \rightarrow \sigma^*$ (C=O)	303.1

resolved. The broad features above the edge belong to  $C\ 1s-\sigma^*$  transitions. To evaluate the data a multi-Gaussian fit was performed. In table 1 the identified features are summarized and compared with reference data obtained from synchrotron experiments.

As can be seen, the obtained energy values of the peaks deviate by less than 0.4 eV from the corresponding synchrotron data.

#### 3.2. NEXAFS in reflection

In order to measure the near-edge fine structure in a transmission experiment the thickness of the sample has to be well adjusted to the absorption length  $1/\mu$  of the material. For thick samples the transmitted signal is low and thickness effects can lead to a distortion of the NEXAFS signal [19]. On the other hand, for thin samples the concentration of the element of interest may be too low to get a sufficient contrast at the absorption edge.

In order to overcome these limitations, advantage can be taken of the fact that the refractive index  $n(\omega) = 1 - \delta + i\beta$  ( $\delta$ : phase shift,  $\beta$ : absorption) is slightly smaller than unity in the XUV range, resulting in total external reflection [21]. Therefore, NEXAFS spectra were recorded at a fixed glancing angle  $\theta = 2^\circ$  below the critical angle  $\theta_c = \sqrt{2\delta}$  ( $\theta_c \approx 3^\circ$  for carbon at  $\lambda = 4.4$  nm). The reference spectrum was recorded by tilting the spectrometer around the axis of the entrance slit in order to detect direct light from the source.

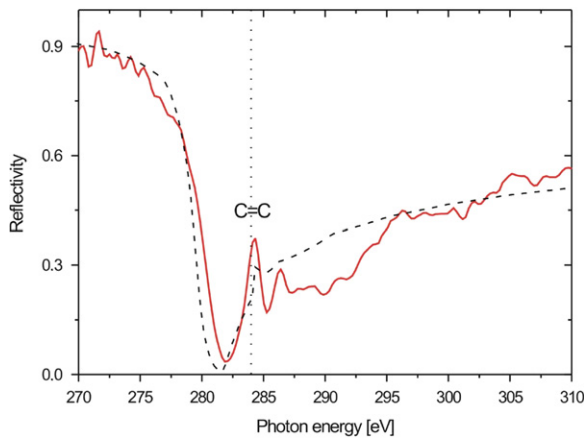


**Figure 5.** Measured reflectivity of polyimide under grazing incidence conditions (angle of incidence to the surface  $2^\circ$ ) as a function of photon energy. The dashed line shows the calculated carbon reflectivity and the dotted line indicates the position of the carbon K-edge (data taken from CXRO [17]).

According to the Fresnel equation the reflectivity for soft x-rays in the case of glancing incidence is given by

$$R = \frac{\left| \theta - \sqrt{(\theta^2 - 2\delta) + 2i\beta} \right|^2}{\left| \theta + \sqrt{(\theta^2 - 2\delta) + 2i\beta} \right|^2}. \quad (2)$$

Since the Fresnel reflectivity is a function of the dispersion  $\delta(E)$  and absorption  $\beta(E)$  that are also energy dependent, the reflected intensity recorded as a function of energy contains the near-edge absorption structure. For incidence angles below the critical angle  $\theta_c$  the reflectivity is mainly influenced by the absorption  $\beta$  but with no pronounced NEXAFS structure. Near the critical angle  $\theta_c$  the reflectivity is influenced by  $\delta$  and  $\beta$ , resulting in strong NEXAFS structures [20].

The field penetration depth  $z_c$  at the critical angle  $\theta_c$  is given by [21]

$$z_c = \frac{\lambda}{2\pi\beta^{\frac{1}{2}}}, \quad (3)$$

being in the range 15–30 nm for carbon at  $\lambda = 4.4$  nm. Thus, the NEXAFS spectra recorded under grazing incidence conditions yield surface sensitive information.

For the measurement of the NEXAFS spectrum in reflection mode the same polyimide film as in the case of transmission was chosen and illuminated under a glancing angle of  $2^\circ$ . The resulting energy dependent reflectivity ( $I_R/I_0$ ) is shown in figure 5.

The reflectivity curve shows strong oscillations above 282 eV that can be attributed to C  $1s-\pi^*$  transitions. Compared with the transmission measurements the peak positions are slightly shifted to lower photon energies due to the influence of the real part of the refractive index [20]. It has also been shown for hard x-rays that the extraction of  $\delta(E)$  and  $\beta(E)$  is possible from these reflectivity measurements [22]. However, this approach is only valid in the case of  $\delta(E) > 0$ . In the case of the carbon K-edge this approach is not applicable, since  $\delta(E)$  also becomes negative.

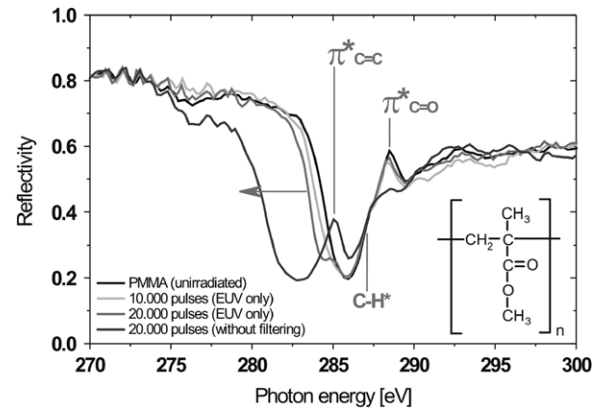


**Figure 6.** Measured XUV reflectivity as a function of photon energy for PMMA, irradiated with different numbers of EUV pulses (angle of incidence to the surface  $2^\circ$ ).

#### 4. Irradiation of PMMA with EUV radiation

In recent papers we have demonstrated the direct modification of surfaces with focused EUV radiation using an EUV Schwarzschild objective, e.g. the generation of colour centres in lithium fluoride [23] and the direct photo etching of PMMA [24]. In particular, the interaction mechanisms between soft x-rays and polymers are of great interest, since for example PMMA is used as a photo resist for EUV lithography [25], as well as for beam profile characterization of free-electron lasers by direct ablation [26].

In order to investigate the interaction of EUV radiation with PMMA, test samples were irradiated at EUV energy densities of  $0.5 \text{ mJ cm}^{-2}$  with different pulse numbers. The radiation induced changes were analysed afterwards using NEXAFS in reflection mode as well as by Fourier transformation infrared (FTIR) spectroscopy. For the FTIR measurements a Bruker IFS 88 IR-spectrometer was used in ATR-mode (attenuated total reflectance). In this case the penetration depth of the evanescent wave is in the range  $0.5\text{--}2.5 \mu\text{m}$  for PMMA [27].

For the experiments, a PMMA plate (Goodfellow, thickness 1 mm) was cut into  $10 \times 10 \text{ mm}^2$  pieces and cleaned in ethanol. The samples were positioned 90 mm next to an EUV plasma (4 mJ, 2% BW,  $4\pi$  sr [24]) and were irradiated with different numbers of EUV pulses. In order to block non-EUV radiation, a zirconium foil (thickness 220 nm) could be positioned in front of the sample, transmitting radiation between 6 and 20 nm ([28], transmission approximately 50% at 13.5 nm).

NEXAFS measurements in reflection mode were carried out on the EUV irradiated samples in the same way as described above. It was checked before that the chemical structure of the sample is not changed during the NEXAFS experiments by recording several NEXAFS spectra of the same sample subsequently. A comparison of the energy dependent reflectivity for PMMA samples irradiated with different EUV pulse numbers is shown in figure 6. The characteristic peaks of the reflectivity can be assigned to C=C and C=O double bonds.

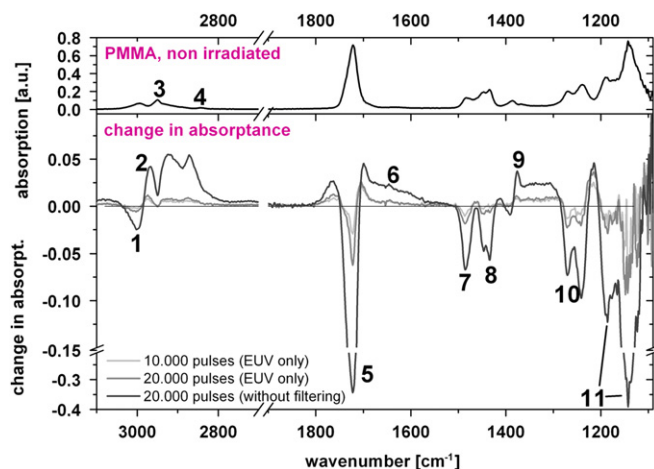


**Figure 7.** FTIR measurements of PMMA samples, irradiated with different numbers of EUV pulses. The spectrum of non-irradiated PMMA is shown on the top; changes due to irradiation with different numbers of EUV pulses are displayed below. The identified absorption edges are compiled in table 2.

It can be seen that with an increasing pulse number the peak height of the C=O bond decreases. This clearly indicates a loss of the carbonyl functional group that is easily radiation damaged [29]. Furthermore, the appearance of a new feature can be observed with increasing radiation dose at 285 eV that corresponds to the C 1s  $\rightarrow \pi_{C=C}^*$  transition. The formation of a C=C double bond, which is not part of the chemical structure of PMMA, after 20,000 EUV pulses is a result of crosslinking upon irradiation [29]. It can be explained by the removal of the ester side chain, which was shown to have a linear stoichiometric relationship (1 : 1) with the formation of a C=C double bond [30]. The shift of the reflectivity minimum with increasing pulse number to lower photon energies can be attributed to a loss of oxygen and hydrogen atoms from the PMMA molecule that is consistent with the process leading to crosslinking [29].

The corresponding FTIR measurements of the same samples are shown in figure 7, with the spectrum of non-irradiated PMMA at the top. The spectral changes due to EUV irradiation of PMMA are displayed below. Negative values indicate a decrease in the corresponding molecular vibration.

In table 2 the identified absorption bands are listed. The FTIR spectrum shows radiation induced changes in every absorption band. The absorption of the C=O bond (peak No 5 in figure 7) is strongly decreased, which is in good agreement with the NEXAFS experiments. The decrease in the skeletal valence vibrations indicates a large fragmentation of the PMMA surface.

In contrast to the NEXAFS measurements the increase in the C=C bond (peak No 6) vibration is only visible for the highest EUV dose. This could be explained by the difference in penetration depths that is about two orders of magnitude larger in the case of the FTIR measurements compared with the NEXAFS method.

The generation of C=C bonds might therefore be a surface-near process, where the EUV dose is very high, whereas the breaking of C=O bonds might be a process in the entire bulk.

**Table 2.** Absorption bands observed in the FTIR spectrum of EUV irradiated PMMA (cf figure 7). The bands were identified by comparison with literature data [31,32]. Denotation of vibrations by Günzler [33]:  $\nu_{s,a}$  symmetrical/asymmetrical stretch vibration,  $\delta$ : deformation vibrations around the valence bond angle.

ID	Wavenumber (cm <sup>-1</sup> )	Classification
1	2993	$\nu_a(\text{CH}_3\text{-O}), \nu_a(\text{CH}_2)$
2	2950–2975	$\nu_a(\alpha\text{-CH}_3)$
3	2950	$\nu_s(\text{CH}_3\text{-O}), \nu_a(\alpha\text{-CH}_3), \nu_s(\alpha\text{-CH}_3), \nu_s(\text{CH}_2)$
4	2920	Combination band, C(=O)O–CH <sub>3</sub>
5	1730	$\nu(\text{C=O})$
6	1643	$\nu(\text{C=C})$
7	1483	$\delta_a(\text{CH}_3\text{-R})$
8	1438	$\delta_s(\text{CH}_3\text{-O})$
9	1370	$\delta_s(\alpha\text{-CH}_3)$ (amorphous)
10	1268, 1238	$\nu_a(\text{C-C-O})$ coupled with $\nu(\text{C-O})$
11	1191, 1145	Skeletal valence vibrations, coupled with inner CH deformation vibrations

## 5. Conclusion

The results presented in this paper demonstrate that it is possible to investigate the near-edge absorption fine structure by utilizing broad-band radiation from a laboratory-scale laser-driven plasma source. NEXAFS spectra obtained from thin polymer films are in good agreement with the respective synchrotron data. The possibility to record NEXAFS spectra in reflection mode under grazing incidence conditions circumvents the need for thin film sample preparation. Moreover, due to the low penetration depth of the soft x-rays, ReflEXAFS data offer a much stronger surface sensitivity (<30 nm) than comparative FTIR data. By using the ReflEXAFS method it was possible to investigate compositional changes of PMMA upon EUV irradiation. The spectra clearly show the loss of the carbonyl functional group as well as crosslinking effects at high EUV radiation doses.

In future, the spectral resolution of the setup shall be improved by using a higher resolution grating. In forthcoming experiments the advantage of the short pulse length of the soft x-ray pulse will be taken in order to perform time-resolved experiments in pump-probe schemes.

## Acknowledgments

The authors would like to thank Uwe Leinhos (Laser-Laboratorium Göttingen) and Jürgen Niemeyer (IBT/Göttingen) for fruitful discussions. The financial support by SFB755 ‘Nanoscale Photonic Imaging’ is acknowledged.

## References

- [1] Jansson P, Vogt U and Hertz H 2005 *Rev. Sci. Instrum.* **76** 043503
- [2] Fiedorowicz H 2005 *Laser Particle Beams* **23** 365–73
- [3] Peth C *et al* 2007 *Rev. Sci. Instrum.* **78** 103509
- [4] Seres J *et al* 2007 *Nature Phys.* **3** 878–83
- [5] Zepf M *et al* 2007 *Phys. Rev. Lett.* **99** 143901

- [6] Wang Y, Granados E and Rocca J J 2006 *Phys. Rev. Lett.* **97** 123901
- [7] Takman P, Stollberg H and Hertz H 2007 *J. Microsc.* **226** 175–81
- [8] Wieland M *et al* 2005 *Ultramicroscopy* **102** 93–100
- [9] Sandberg R *et al* 2007 *Phys. Rev. Lett.* **99** 098103
- [10] Kondo H, Tomie T and Shimizu H 1996 *Appl. Phys. Lett.* **69** 182
- [11] Vogt U, Wilhein T, Stiel H and Legall H 2004 *Rev. Sci. Instrum.* **75** 4606
- [12] Stöhr J 2003 *NEXAFS Spectroscopy (Springer Series in Surface Science vol 25)* (Berlin: Springer)
- [13] Dhez O, Ade H and Urquhart G S 2003 *J. Electron Spectrosc. Relat. Phenom.* **128** 85–96
- [14] Beck M *et al* 2001 *Opt. Commun.* **190** 317
- [15] Kranzusch S, Peth C and Mann K 2003 *Rev. Sci. Instrum.* **74** 969
- [16] NIST Atomic Spectra Database, <http://physics.nist.gov/PhysRefData/ASD/index.html>
- [17] Center for X-Ray Optics <http://www-cxro.lbl.gov/>
- [18] Jordan-Sweet J L *et al* 1988 *J. Chem. Phys.* **89** 2482–9
- [19] Stern A E and Kim K 1981 *Phys. Rev. B* **23** 3781–7
- [20] Martens G and Rabe P 1981 *J. Phys. C: Solid State Phys.* **14** 1523–34
- [21] Attwood D 1999 *Soft X-Rays and Extreme Ultraviolet Radiation* (Cambridge: Cambridge University Press)
- [22] Tani K *et al* 2004 *Spectrochim. Acta B* **59** 1221–5
- [23] Barkusky F *et al* 2005 *Rev. Sci. Instrum.* **76** 105102
- [24] Barkusky F, Peth C, Bayer A and Mann K 2007 *J. Appl. Phys.* **101** 124908
- [25] He D *et al* 1999 *J. Vac. Sci. Technol. B* **17** 3379
- [26] Chalupsky J *et al* 2007 *Opt. Express* **15** 6036
- [27] Pedrotti F and Pedrotti L 1993 *Introduction to Optics* 2nd edn (Englewood Cliffs, NJ: Prentice-Hall)
- [28] Kranzusch S, Peth C and Mann K 2003 *Rev. Sci. Instrum.* **74** 969
- [29] Coffey T, Urquhart G S and Ade H 2002 *J. Electron Spectrosc. Relat. Phenom.* **122** 65
- [30] Choi J *et al* 1988 *J. Vac. Sci. Technol B* **6** 2286
- [31] Dechant J 1972 *Ultrarotspektroskopische Untersuchung an Polymeren* (Berlin: Akademie)
- [32] Willis A H, Zichy V J I and Hendra J P 1969 *Polymer* **10** 737
- [33] Günzler H and Heise M H 1996 *IR-Spektroskopie* (Weinheim: VCH)